Supplementary Information

Sandwich Structured WO_3 Nanoplatelets for Highly Efficient Photoelectrochemical Water Splitting

Guangwei Zheng,[a,b] Jinshu Wang,*[a] Guannan Zu,[a] Haibing Che,[a] Chen Lai,[a] Hongyi Li,[a]

Vignesh Murugadoss,[b,c,d] Chao Yan,[e] Jincheng Fan,[f] and Zhanhu Guo*[b]

[a] *Key Lab of Advanced Functional Materials, Ministry of Education, College of Materials Science and Engineering, Beijing University of Technology, Beijing 100124, China. Email: wangjsh@bjut.edu.cn*

[b] *Integrated Composites Laboratory (ICL), Department of Chemical & Biomolecular Engineering, University of Tennessee, Knoxville, TN 37996, United States. E-mail: zguo10@utk.edu*

[c] *Key Laboratory of Materials Processing and Mold (Zhengzhou University), Ministry of Education, National Engineering Research Center for Advanced Polymer Processing Technology, Zhengzhou University, Zhengzhou, 450002, Henan, China*

[d] *School of Materials Science and Engineering, North University of China, Taiyuan 030051, China*

[e] *School of Materials Science and Engineering, Jiangsu University of Science and Technology, Zhenjiang 212003, China E-mail: chaoyan@just.edu.cn*

[f] *College of Materials Science and Engineering, Changsha University of Science and Technology,Changsha 410114, China E-mail: fanjincheng2009@163.com*

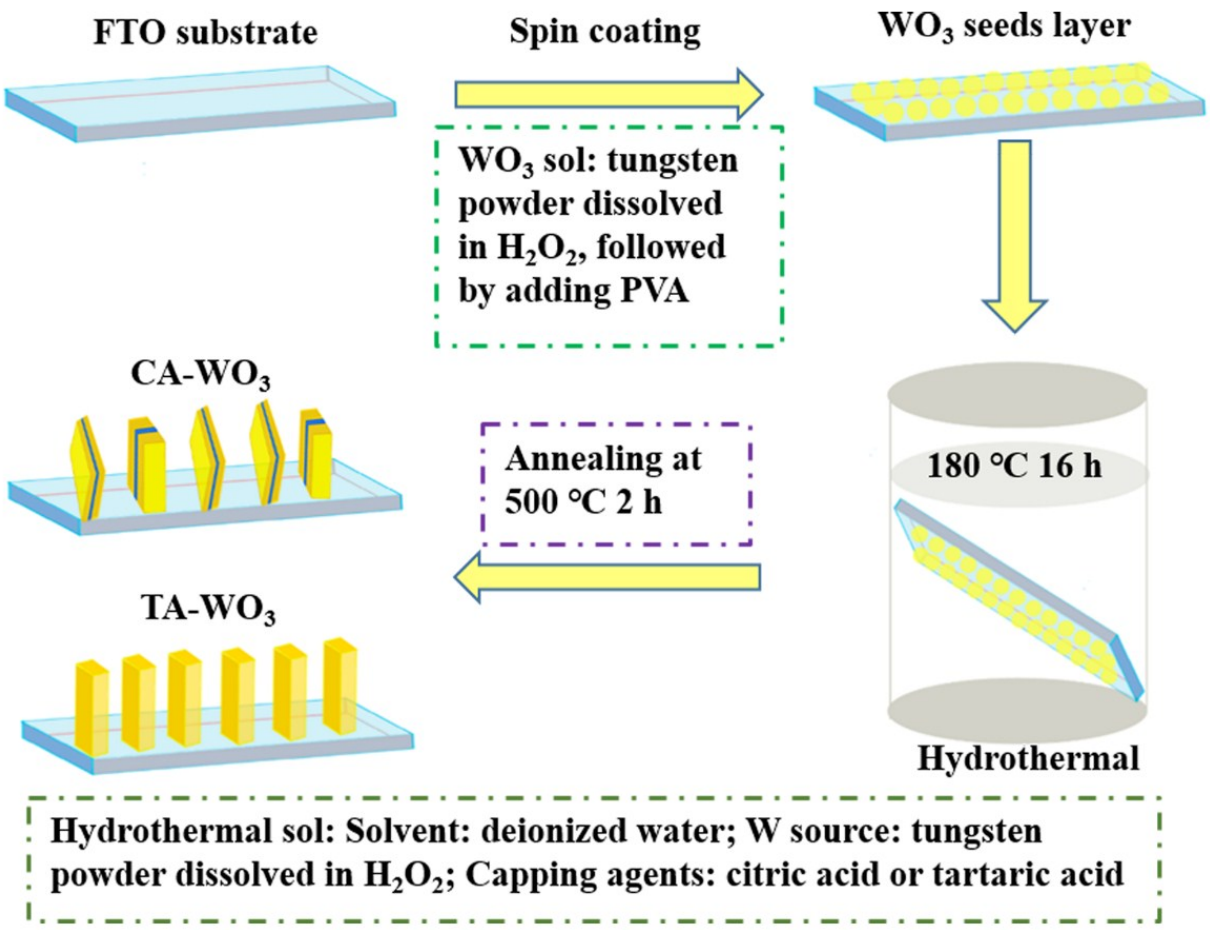

Scheme S1. Schematic illustration of the forming process for CA-WO_3 and TA-WO_3 photoanodes films by a facile hydrothermal method without using HCl/ or a hazardous chemical

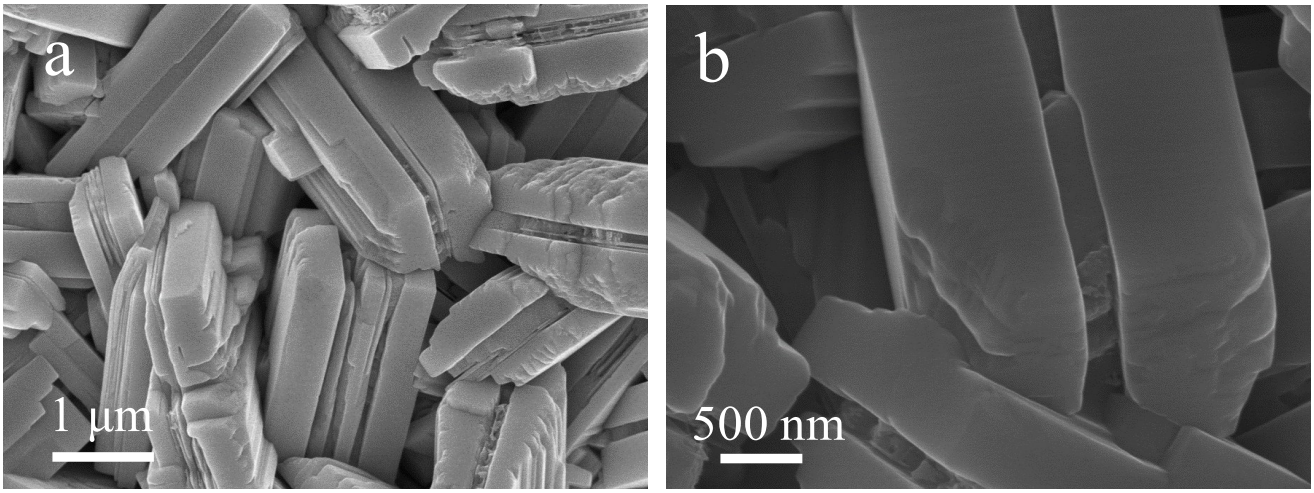

Fig. S1 The high resolution SEM images of the CA-WO_3.

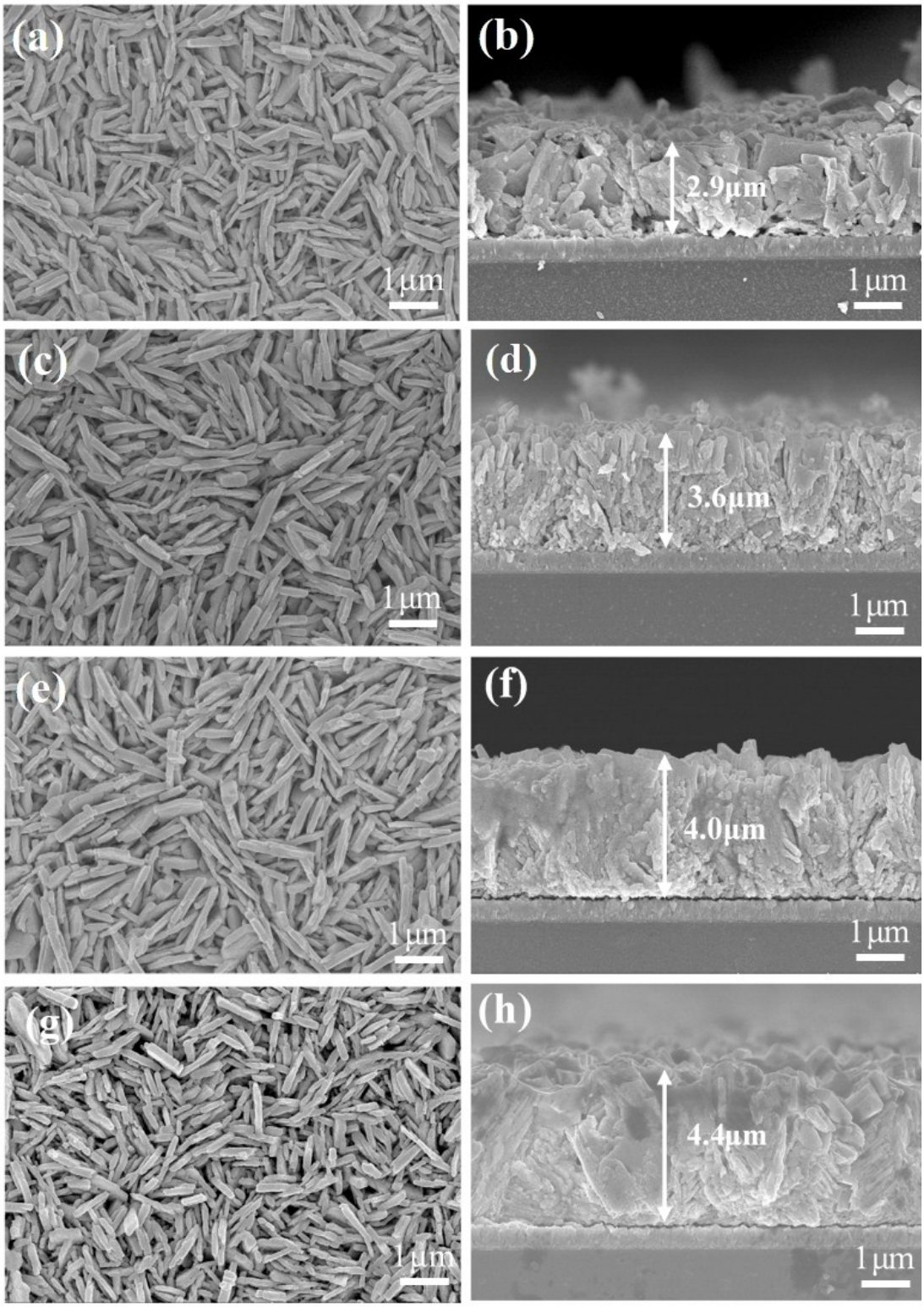

Fig. S2 (a, c, e, g) Top-view and (b, d, f, h) side-viewed SEM images of TA-WO_3 samples obtained at hydrothermal treatments for 4 h, 8 h, 12 h, 16 h respectively, followed by annealed at 500 ^{o}C for 2 h.

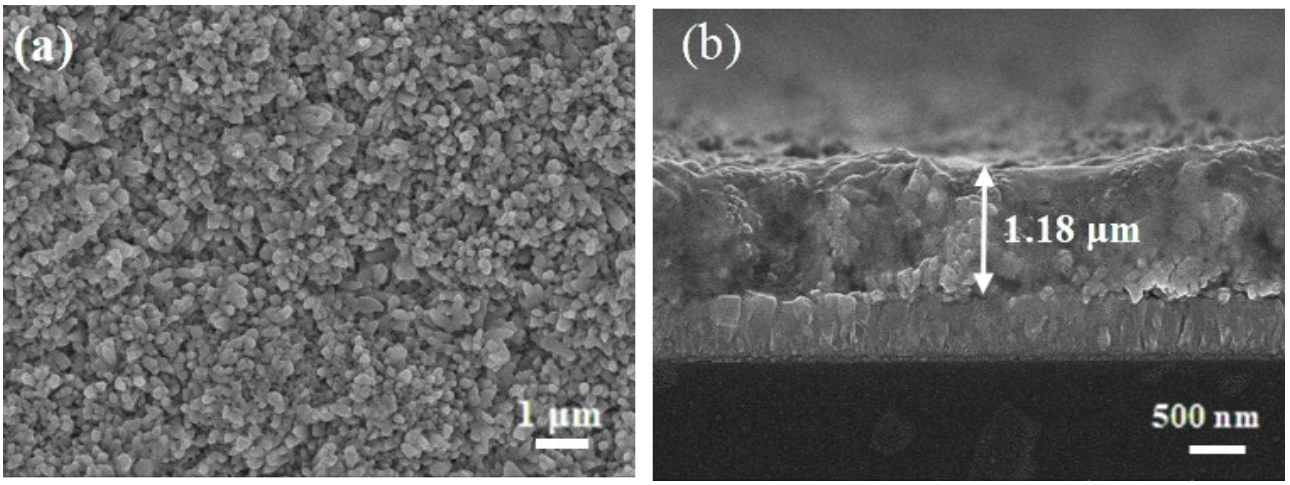

Fig. S3 (a) Top-view and (b) side-viewed SEM image of the WO_3 photoanodes films grown on FTO substrate at 180 ^oC for 12 h without a capping agent

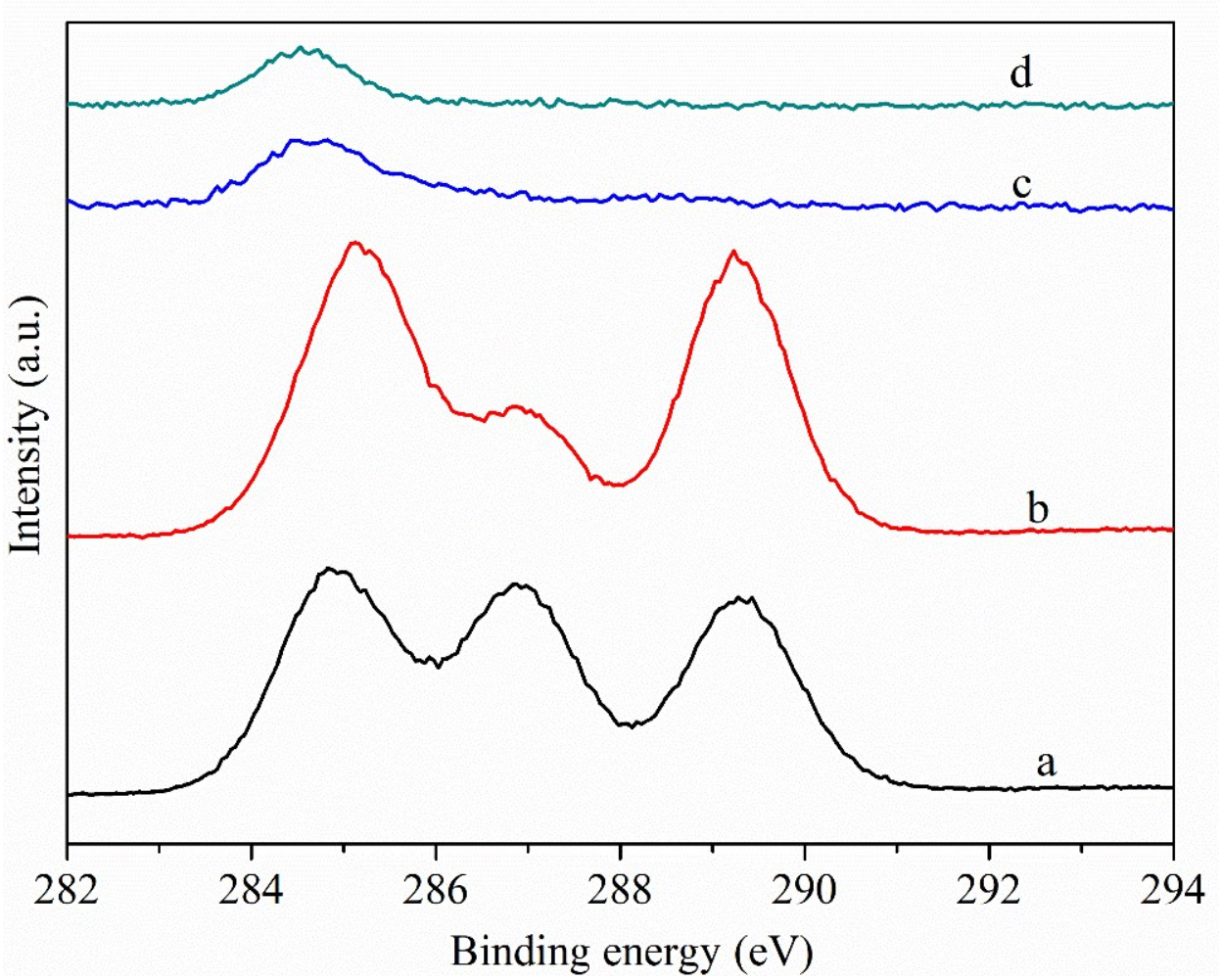

Fig. S4 The C1s XPS-peak of (a) pure tartaric acid, (b) pure citric acid, (c) TA-WO_3 and (d) CA-WO_3 photoanodes prepared at hydrothermal treatment for 16 h followed by annealed at 500 ℃ for 2 h.

In the process of preparation of WO_3, we used deionized water to wash the WO_3 film after the hydrothermal treatment. After that, most of the organic ligands could be removed. Moreover, the WO_3 films were further annealed at 500 ℃ for 2 h in the air at a heating rate of 2 °C/min, the tartaric acid and citric acid are completely decomposed under the high calcination-temperature. To prove this point, we provided the C1s XPS-peak of pure tartaric acid, citric acid, TA-WO_3 and CA-WO_3 prepared at hydrothermal treatment for 16 h followed by annealed at 500 ℃ for 2 h, as shown in Fig. S4. It is clear that the C1s peak of the pure tartaric acid and citric acid exhibit strong characteristic peaks at around 284.9-289.2 eV which correspond to C-C, C-H, C-O, and O-C=O bonds. Whereas, the TA-WO_3 and CA-WO_3 photoanodes showed an only peak at 284.7 eV which can be attributed to CO_2 adsorbent on the surface of WO_3. Therefore, no organic ligands are residual on the surface of the obtained WO_3.

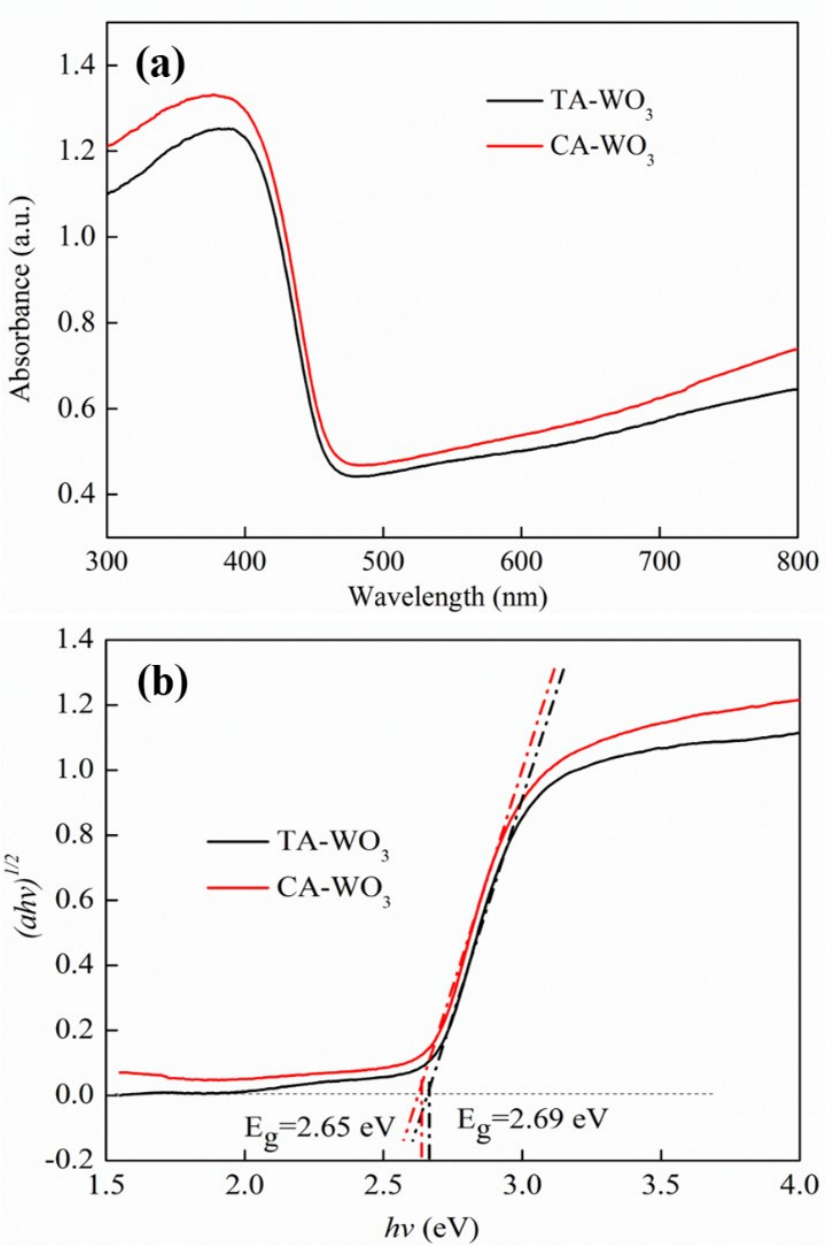

Fig. S5 (a) UV-visible absorption spectra and (b) corresponding Tauc plots of CA-WO_3-12h and TA-WO_3-16h.

The optical band gap of CA-WO_3-12h and TA-WO_3-16h could be determined by the equation $\alpha h\upsilon = A(h\upsilon - E_g)^n$, where α, h, υ are the absorption coefficient, Planck's constant, and frequency of light, respectively, and A, E_g, n are constant related of material, band gap energy, and n equals to 2 for WO_3 as an indirect semiconductor, respectively. Therefore, the band gap energy for the WO_3

products are obtained for the plotted $(\alpha h\upsilon)^{1/2}$ as a function of $h\upsilon$. According to the Tauc plots, the energy band gaps of CA-WO_3-12h and TA-WO_3-16h are estimated to be 2.65 and 2.69 eV, respectively.

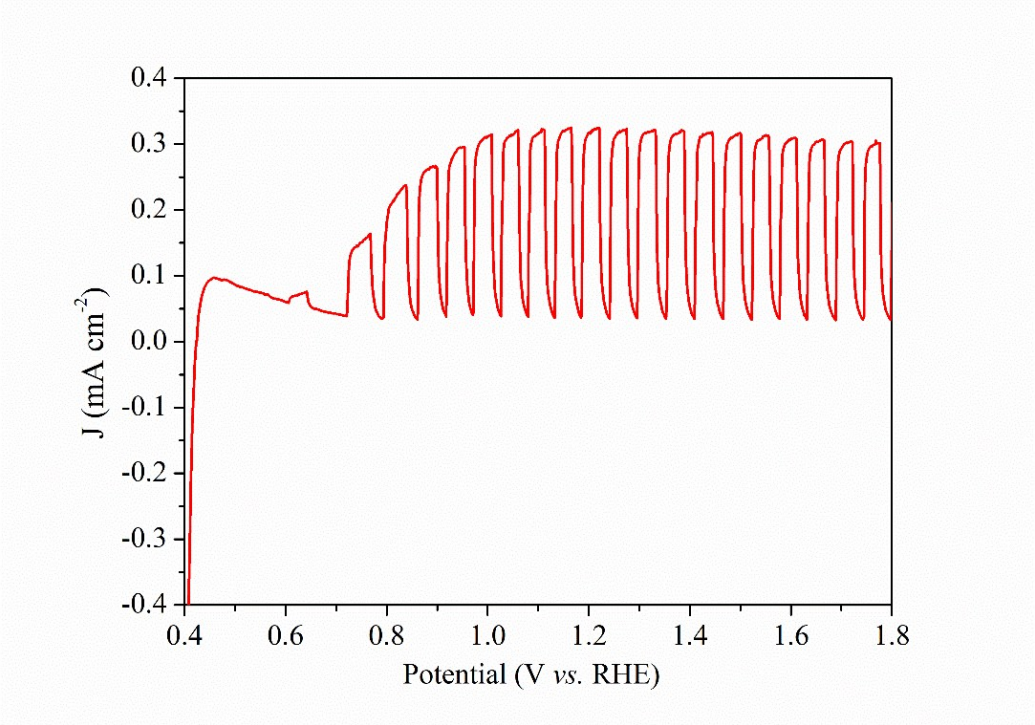

Fig. S6 Chopped photocurrent-potential (J-V) plots of WO_3 photoanode fabricated without capping agent.

As shown in Fig. S3, the WO_3 photoanodes synthesized without capping agent were composed of nanoparticles and exhibited the photocurrent density of 0.33 mA cm^{-2} at 1.23 V *vs* RHE (Fig. S6). This value is much lower compared with the TA-WO_3. A large number of grain boundaries in the nanoparticle films result in increasing resistance and interfacial charge recombination, thus impeding the electron transfer to the back-contacted conductive. Different from WO_3 photoanodes (without capping agent), the TA-WO_3 electrodes were composed of plate-like structure that were nearly perpendicular grown on FTO substrate. Due to the direct electrical pathways for photogenerated carriers, 2-D plate-like structure can efficiently facilitate the transportation of photoelectrons to FTO and thus suppresses the recombination of photogenerated electron-hole pairs. This structures are capable of reducing grain boundaries and defects that result in less

recombination of electron-hole pairs, and consequently 2-D TA-WO_3 photoanodes demonstrated superior PEC properties compared to nanocrystalline particles.

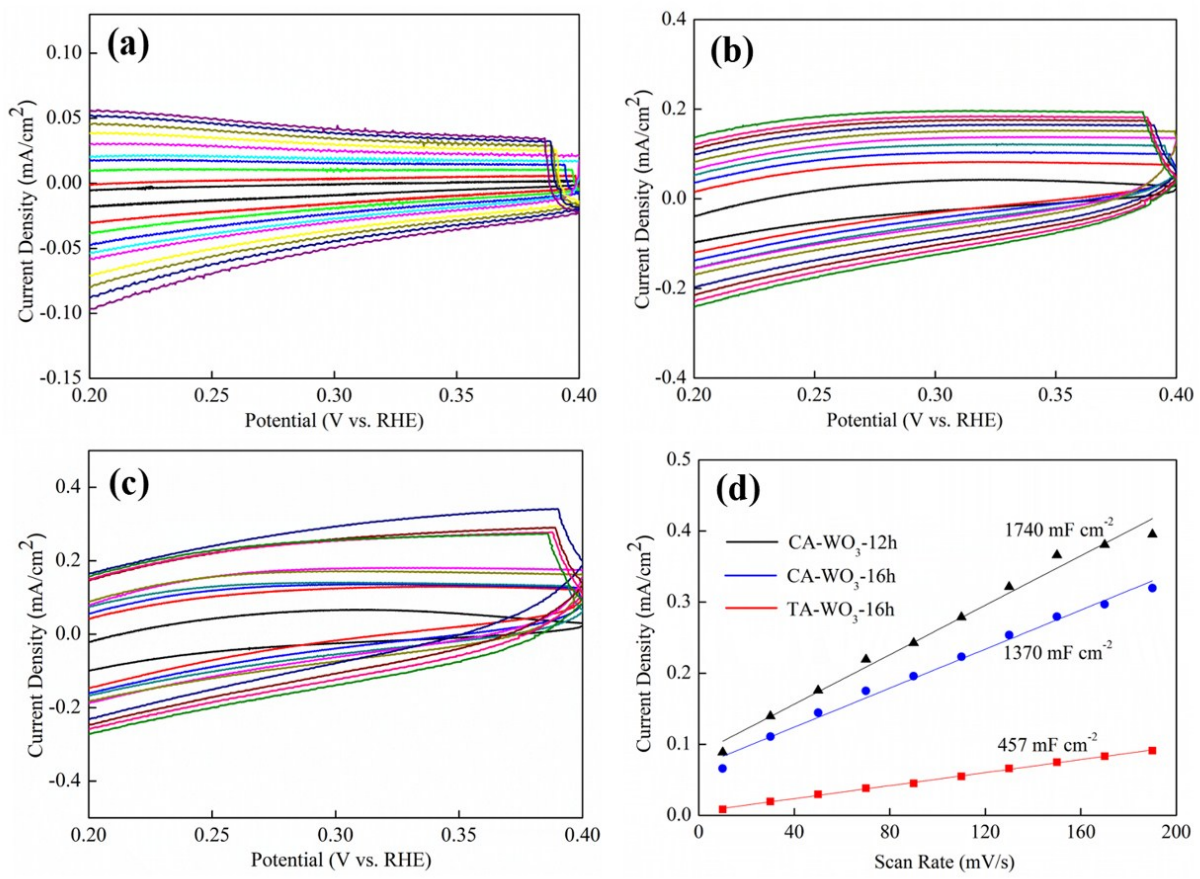

Fig. S7 Electrochemical surface area analysis for the three samples in the non-faradaic region at different scan rates, varying from 10 mV s^{-1} to 190 mV s^{-1}: (a) TA-WO_3-16h, (b) CA-WO_3-16h, (c) CA-WO_3-12h, (d) scan rate dependence of the current densities.

Table S1 XRD peak intensity ratios of (002) to (200) of different samples

samples	$I_{(002)}/I_{(200)}$
CA-WO_3-4h[a]	0.62
CA-WO_3-8h[b]	0.99
CA-WO_3-12h[c]	1.31
CA-WO_3-16h[d]	1.68

[a][b][c][d] CA-WO_3 samples obtained at hydrothermal treatments for 4 h, 8 h, 12 h, 16 h, respectivly, followed by annealing at 500 ^oC for 2 h

Table S2 EIS fitting results of R_{ct} for CA-WO_3-12h, CA-WO_3-16h, and TA-WO_3-16h photoanodes

Samples	R_s (Ω)	%error	R_{ct} (Ω)	%error	C (mF)	%error
CA-WO_3-12h[a]	19.52	3.34	570	3.09	14.39	4.45
CA-WO_3-16h[b]	20.02	2.70	1041	2.39	9.90	3.19
TA-WO_3-16h[c]	27.06	6.01	1213	5.51	9.57	7.42

[a][b] CA-WO_3 samples obtained at hydrothermal treatments for 12 h and 16 h, respectivly, followed by annealed at 500 ^oC for 2 h

[c] TA-WO_3 samples obtained at hydrothermal treatments for 16 h, followed by annealed at 500 ^oC for 2 h

Table S3 An overview of representative WO_3 photoanodes reported for efficient photoelectrochemical water splitting

Preparation method	Morphology (thickness of film)	Electrolyte	J (mA cm^{-2}) (applied potential)	IPCE (%)	Ref
Solvothermal	Nanoplates(850 nm)	0.1 M Na_2SO_4	1.42 (1.23 V vs. RHE	~38 (400 nm at 1.23V vs RHE)	1
Solvothermal	Flake-like(3.6 μm)	0.1 M Na_2SO_4	~1.9 (1.2 V vs. Ag/AgCl)	~36 (400 nm at 1.2 V vs Ag/AgCl)	2
Solvothermal	Nanosheet(2 μm)	0.1 M Na_2SO_4	1.62 (1.25 V vs. Ag/AgCl)	~20 (400 nm at 0.67 V vs Ag/AgCl)	3
Solvothermal	Nnanoflake (5.6μm)	0.1 M Na_2SO_4	1.43 (1.23 V vs. RHE)	~70% (480 nm at 1.23 V *vs.* RHE)	4
Hydrothermal	Nanoplate (2.3 μm)	0.5 M Na_2SO_4	1.88 (1.3 V vs. Ag/AgCl)	~65 (1.0 V vs. Ag/AgCl)	5
Glancing angle deposition	Nanorod (3 μm)	0.5 M KPi +1M Na_2SO_3	2.15 (1.23 V vs. RHE)	40 (385 nm at 1.23 V vs. RHE)	6
Hydrothermal	Nanoflakes (1.2 μm)	0.1 M Na_2SO_4	2.49 (1.23 V vs. RHE)	23.25 (440 nm at 1.23 V vs. RHE)	7
Hydrothermal	Tree-like nanoarrays (1.2 μm)	0.5 M Na_2SO_4	1.35 (1.23 V vs. RHE)	\	8
Polymer-assisted deposition	Nanoparticles	0.1 M KPi butter	1.45 (1.23 V vs. RHE)	\	9
Seed-mediated hydrothermal	Microplates (2.4 μm)	0.1 M Na_2SO_4	1.9 (0.6 V *vs.* Ag/AgCl)	\	10
Hydrothermal	Nanorods (800 nm)	0.5 M H_2SO_4	2.26 (1.23 V vs. RHE)	~90% (350 nm at 1.23 V *vs*. RHE)	11
Pulsed laser deposition (PLD)	Tree-like nanoporous (3.2 μm)	0.5 M KPi + 0.5 M H_2SO4	1.8 (1.23 V vs. RHE)	78% (350 nm at 1.23 V *vs*. RHE	12
Hydrothermal	Microcrystals	1 M H_2SO_4	0.45 (0.8 V *vs.* RHE)	~2.7% (300 nm at 0.8 V *vs*. RHE)	13
Hydrothermal	Nanoparticles (2.9 μm)	0.5 M H_2SO_4	2.7 mA (1.4 V *vs.* RHE)	\	14
Pulsed laser deposition (PLD)	Nanoneedles (17.6 μm)	0.1 M H_2SO_4	2.4 (1.23 V vs. RHE)	50% (410 nm at 1.23 V *vs*. RHE)	15
Solvothermal	Nanoflakes (3 μm)	0.1 M Na_2SO_4	1.1 (1.23 V *vs.* RHE)	~45% (320 nm at 1.23 V *vs*. RHE)	16

Table S3 (continued)

Preparation method	Morphology (thickness of film)	Electrolyte	J (mA cm^{-2}) (applied potential)	IPCE (%)	Ref
Hydrothermal	Nanoplates (1.3 μm)	0.2 M Na_2SO_4	1.6 (1.2 V *vs.* Ag/AgCl)	55% (355 nm at 1.0 V *vs*. Ag/AgCl)	17
PLD	Nano-tree like (10 μm)	1 M H_2SO_4	1.85 (0.8 V vs. RHE)	63 (400 nm at 1.0 V vs. RHE)	18
Hydrothermal	Nanorods (1.5 μm)	0.5 M Na_2SO_4	1.05 (1.1 V vs. SCE)	\	19
Hydrothermal	Nanoplates (2 μm)	1 M H_2SO_4	1.2 (1.23 V. vs. RHE)	40 (350 nm at 1.23 V vs. RHE)	20
Hydrothermal	Nanoplates (4.4 μm)	0.1 M Na_2SO_4	3.16 (1.23 V vs. RHE)	79 (400 nm at 1.23 V vs. RHE)	This work

RHE: reversible hydrogen electrode; SCE: saturated calomel electrode

References

1 Q. Y. Zeng, J. H. Li, J. Bai, X, J. Li, L. G. Xia, B. X. Zhou, *Appl. Catal. B: Environ*., 2017, **202**, 388–396

2 F. Amano, D. Li, B. Ohtani, Chem. Commun., 2010, **46**, 2769–2771

3 J. J. Zhang, P. Zhang, T. Wang, J. L. Gong, Nano Energy, 2015, **11**, 189–195

4 J. Z. Su, X. J. Feng, J. D. Sloppy, L. J. Guo, C. A. Grimes, Nano Lett., 2011,**11**, 203–208

5 X. Y. Feng, Y. B. Chen, Z. X. Qin, M. L. Wang, L. J. Guo, ACS Appl. Mater. Interfaces, 2016, **8**, 18089−18096

6 M. G. Lee, D. H. Kim, W. Sohn, C. W. Moon, H. Park, S. H. Lee, H. W. Jang, Nano Energy, 2016, **28**, 250–260

7 J. J. Zhang, X. X. Chang, C. C. Li, A. Li, S. S. Liu, T. Wang, J. L. Gong, J. Mater. Chem. A, 2018, **6**, 3350–3354

8 R. K. Zhang, F. Y. Ning, S. M. Xu, L. Zhou, M. F. Shao, M. Wei, Electrochimica Acta, 2018, **274**, 217–223

9 J. H. Kim, B. J. Lee, P. Wang, M. H. Son, J. S. Lee, Appl. Catal. A: Gen., 2016, **521**, 233–239

10 M. Park, J. H. Seo, H. Song, K. M. Nam, J. Phys. Chem. C, 2016, **120**, 9192−9199

11 S. S. Kalanur, Y. J. Hwang, S. Y. Chae, O. S. Joo, J. Mater. Chem. A, 2013, **1**, 3479−3488

12 S. Shin, H. S. Han, J. S. Kim, I. J. Park, M. H. Lee, K. S. Hong, I. S. Cho, J. Mater. Chem. A, 2015, **3**, 12920–12926

13 J. Zhang, Z. H. Liu, Z. F. Liu, ACS Appl. Mater. Interfaces, 2016, **8**, 9684−9691

14 W. Z. Li, J. Li, X. Wang, J. Ma, Q. Y. Chen, Int. J. Hydrogen Energy, 2010, **35**, 13137–13145

15 C. Fàbrega, S. Murcia-López, D. Monllor-Satoca. J.D. Prades, M.D. Hernández-Alonso, G. Penelas, J.R. Morante, T. Andreu, Appl. Catal. B: Environ., 2016, **189**, 133–140

16 C. W. Wang, C. F. Tang, X. Y. Zhang, L. Qian, H. G. Yang, Prog. Nat. Sci-Mater., 2018, **28**, 200–204

17 W. H. Liu, Y. H. Yang, F. Q. Zhan, D. W. Li, Y. M. Li, X. D. Tang, W. Z. Li, J. Li, Int. J. Hydrogen Energy, 2018, **43**, 8770–8778

18 M. Balandeh, A. Mezzetti, A. Tacca, S. Leonardi, G. Marra, G. Divitini, C. Ducati, L. Meda, F. Di Fonzo, J. Mater. Chem. A, 2015, **3**, 6110–6117

19 Y. Liu, L. Zhao, J. Z. Su, M. T. Li, L. J. Guo, ACS Appl. Mater. Interfaces 2015, **7**, 3532–3538

20 H. Y. Wu, M. Xu, P. M. Da, W. J. Li, D. S. Jia, G. F. Zheng, Phys. Chem. Chem. Phys., 2013, **15**, 16138–16142